AMERICAN ACADEMY OF OPHTHALMOLOGY®

Automatic Measurement and Comparison of Normal Eyelid Contour by Age and Gender Using Image-Based Deep Learning

Ji Shao, MD, Jing Cao, MD,* Changjun Wang, MD, Peifang Xu, MD, Lixia Lou, MD, PhD, Juan Ye, MD, PhD*

Purpose: This study aimed to propose a fully automatic eyelid measurement system and compare the contours of both the upper and lower eyelids of normal individuals according to age and gender.

Design: Prospective study.

Participants: Five hundred and forty healthy Chinese aged 0 to 79 years in a tertiary hospital were included.

Methods: Facial images in the primary gazing position were used to train and test the proposed automatic system for eye recognition and eye segmentation. According to the 10-millimeter diameter circular marker, measurements were transformed from pixel sizes into factual distances.

Main Outcome Measures: Midpupil lid distances (MPLDs) every 15° of all participants were automatically measured in both genders (30 males and 30 females in each age group) by the proposed deep learning (DL)-based system. Intraclass correlation coefficients (ICCs) were performed to assess the agreement between the automatic and manual margin reflex distances (MRDs). The eyelid contour, eyelid asymmetry, and palpebral fissure obliquity were analyzed using MPLD, temporal-versus-nasal MPLD ratio, and the angle between the inner and outer canthi, respectively.

Results: The measurement of MRDs by the automatic system excellently agreed with that of the expert, with ICCs ranging from 0.863 to 0.886. As the age of the participants increased, the values of MPLDs reached a peak in those in their 20s or 30s and then gradually decreased at all angles. The temporal sector showed greater changes in MPLDs than the nasal sector, and the changes were more significant in females than in males. The maximum value of palpebral fissure obliquity appeared before 10 years in both genders and remained relatively stable after the 20s ($P > 0.05$).

Conclusions: The proposed DL-based eyelid analysis system allowed automatic, accurate, and comprehensive measurement of the eyelid contour. The refinement of eyelid shape quantification could be beneficial for future objective assessment preocular and postocular plastic surgery.

Financial Disclosure(s): The authors have no proprietary or commercial interest in any materials discussed in this article. *Ophthalmology Science 2024;4:100518*

Supplemental material available at www.ophthalmologyscience.org.

The normal eyelid position and contour are the basis of the diagnosis of eyelid disorders and assessment of surgery efficacy. For unilateral eyelid abnormality, the contour of the normal fellow eye could be used as a guide during oculoplastic surgery. For bilateral eyelid surgery, the average contour of normal eyelids provides objective reference values. However, eyelid morphology measurements vary according to age, gender, and ethnicity.[1] Previous studies demonstrated the contradictory relationship between age, gender, and eyelid anthropometric results (such as palpebral fissure length and obliquity).[1–3] Furthermore, the assessment of eyelid contour using midpupil lid distance (MPLD) was often focused on the upper eyelid of adults.[4–6] There is a lack of comprehensive eyelid contour measurements which contain both upper and lower eyelids in different genders of all ages.

Recent studies made efforts to quantify eyelid contour on digital facial images.[7–9] With the rapid development of computer technology, the methods for eyelid contour quantification have transitioned from labor-intensive, manual, or semiautomatic approaches that were prone to subjective bias to highly automatic measurement techniques. Deep learning (DL), a hot branch of machine learning, possesses the ability to automatically extract features of input images without manual intervention. It has reached advanced segmentation performance in ophthalmic images.[10–12] In our previous work, we developed an automatic eyelid analysis system to measure the eyelid parameters of patients with thyroid-associated ophthalmopathy and normal participants.[13] The automatic measurements demonstrated high reliability but the sample size was

https://doi.org/10.1016/j.xops.2024.100518
ISSN 2666-9145/24

relatively limited. To further quantify the shape of normal eyelids and establish an objective and comprehensive reference for surgical assessment, here we proposed a fully automatic eyelid analysis system to measure the upper and lower eyelid contours of 540 normal Chinese aged 0 to 79 years and compared these contour differences according to gender and age groups.

Methods

Participants

This prospective study included consecutive healthy participants who visited the Department of Ophthalmology at a single institution for vision screening between July 2020 to November 2021. The eyelid morphology of these participants was evaluated and confirmed as normal by an oculoplastic surgeon with >15 years of experience. The exclusion criteria were as follows: (1) eyelid diseases (ptosis, myasthenia gravis, blepharospasm, eyelid retraction, etc.); (2) a history of eye injury; (3) strabismus; (4) abnormality of cornea and pupil; and (5) previous surgery of eyelid and cornea.

A total of 540 healthy Chinese men and women aged 0 to 79 years were included in this study. All these participants were divided into 9 groups based on their ages and each group included 30 men and 30 women.

This study followed the principles of the Declaration of Helsinki and was approved by the Ethic Committees of the Second Affiliated Hospital of Zhejiang University, School of Medicine (No. 2020-583). Written informed consent was obtained from all adults and guardians of minors.

Image Acquisition

All facial images were taken by a digital camera (Canon 1500 D, Canon Corporation) when participants gazed at the primary position. The camera was fixed on a tripod and positioned 1 meter in front of participants at eye level. All images were taken under the same lighting conditions. A red marker with a 10-mm diameter was attached to the forehead of participants as a reference for transferring the pixel values of measurement into the distance in reality.

Manual Measurement

The manual measurements of margin reflex distance (MRD) of each participant were conducted by an oculoplastic expert with >15 years of clinical experience in accordance with the measurement methods proposed by Putterman.[14] With a penlight held between the examiner's eyes and directed at the patients, MRD 1 and 2 were the vertical measurements from the corneal light reflex to the upper and lower eyelid margin at the primary gazing position, respectively. The expert who performed manual measurement was blinded to the automatic results.

Automatic Eyelid Contour Measurement System Based on DL

Recurrent residual convolutional neural networks with attention gate connection based on U-Net[15] were trained in this study for eye identification and segmentation. U-Net is a popular subset of DL, showing the advantages of segmenting small targets from medical images, and has proven its effectiveness in lesion segmentation of diabetic retinopathy, glaucoma, and oculoplastic diseases.[16–18] In this study, we replaced the traditional convolutional block in each layer with the recurrent residual convolutional unit, which provided a higher accuracy in the refined segmentation of challenging areas than that of the traditional U-Net structure. Figure 1 shows the workflow of the automatic eyelid contour analysis system.

Step 1: Automatic Eye Identification. A total of 60 000 eyes from 30 000 individuals' facial images with eye location labels were extracted from the CelebFaces Attributes Dataset.[19] These images were used to train an eye identification model based on the first-stage recurrent residual convolutional neural networks with attention gate connection based on U-Net. The parameters of employed networks were as follows: input image size = 512 × 512 pixels; epoch = 200; batch size = 4; logistic loss function: BCE loss; optimizer: Adam (lr = 0.00001).

Step 2: Automatic Eye Segmentation. A total of 1862 facial images from 1862 healthy individuals visiting the Second Affiliated Hospital were included. Two senior ophthalmologists delineated the outline of the cornea and eyelid. These images with eye annotations were utilized to train the eye segmentation model on the second-stage recurrent residual convolutional neural networks with attention gate connection based on U-Net. The parameters of the proposed networks were as follows: input image size = 256 × 256 pixels; epoch = 200; batch size = 4; logistic loss function: L1 loss; optimizer: Adam (lr = 0.00001).

Step 3: Prediction of New Images. The facial images of 540 healthy participants consisted of the test set. The average of cornea and eyelid annotations manually delineated by 2 senior ophthalmologists were regarded as the ground truth. The cornea and eyelid boundaries that were outputted by R2U-Net were automatically smoothed by the locally weighted smoothing algorithm to obtain the final masks.

Step 4: Eyelid Contour Measurement. The MPLDs were calculated automatically based on the masked images (Fig 2). After 3 points of corneal limbus were randomly selected to fit a circle, the center of this circle was defined as the pupil center. Because the human cornea is not a perfect circle, this process was repeated 2000 times to finally locate the pupil center using the MeanShift with a Gaussian kernel.[20] Twelve radial lines oriented from the pupil center were drawn automatically. Each line intersected the eyelid border and the pixel distance from the pupil center to each intersection was recorded as $P_{0/15/30/45\ldots\ldots330/345}$, which was calculated to quantitatively describe the eyelid contour (Fig 2A). The utmost pixels of the eyelid border were identified as inner and outer canthi for distinguishing the upper and lower eyelid. The angle between the inner and outer canthi was noted as α (palpebral fissure obliquity, Fig 2B).

Step 5: Pixel Size Calculation. Threshold segmentation of the 10-mm diameter circular marker that was attached to the patient's forehead was applied. The automatic measurements of eyelid contour were then converted from pixel size into the distance in reality according to the millimeter/pixel ratio (R) as follows:

$$\mathrm{MPLD}_{0/15/30/45\ldots\ldots330/345} = \mathrm{P}_{0/15/30/45\ldots\ldots330/345} \times \mathrm{R} \quad (1)$$

Step 6. Step 4 and step 5 were repeated once and the average values of MPLDs and α were recorded as the final results of automatic eyelid contour measurements.

Statistical Analyses

The accuracy of automatic eyelid and cornea segmentation was evaluated by the Dice coefficients, which quantified the similarity of manual annotations and automatic segmentations. The left eye of each participant was included for statistical analysis in this study. Intraclass correlation coefficients (ICCs) were performed to quantize the agreement between automatic and manual MRD measurements, and 2 repeated automatic MRD measurements. The agreement was considered moderate if $0.41 < \mathrm{ICC} \leq 0.60$,

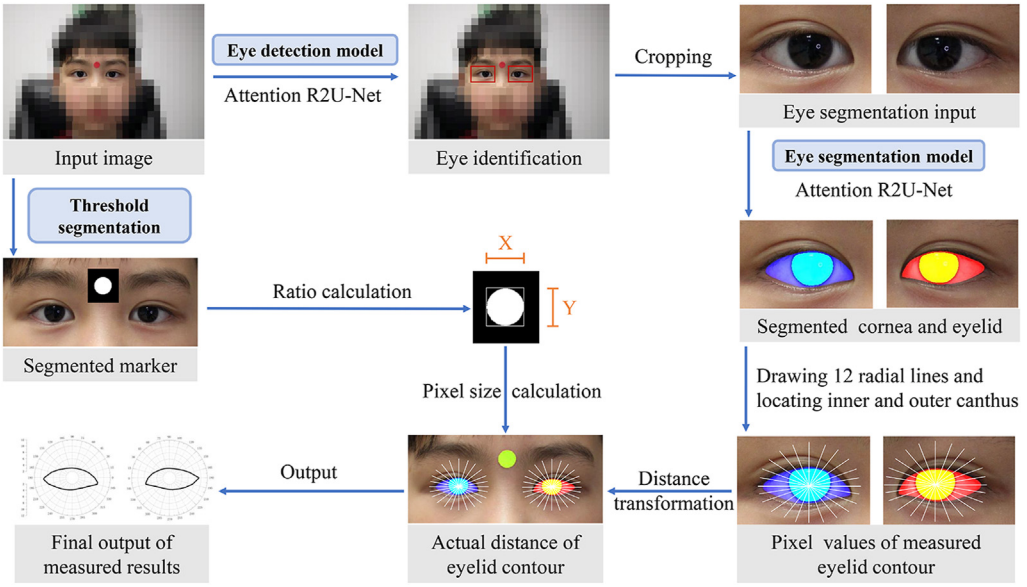

Figure 1. The workflow of the proposed automatic eyelid contour analysis system. Facial images at the primary gazing position were inputted into the deep learning-based eyelid system and 2 models based on Attention R2U-Net (recurrent residual convolutional neural networks with attention gate connection based on U-Net) were used for automatic eye identification and segmentation. Then, this proposed system calculated the pixel values of midpupil lid distances and located the inner and outer canthus. For distance transformation, the 10-millimeter diameter red marker attached to the forehead of each participant was segmented and the system transformed the pixel values into the actual distance using the millimeter-to-pixel ratio. The values of eyelid contour in the real world were outputted as the final results. This image has been published with the consent of the participant's guardian.

substantial if $0.60 < \text{ICC} \leq 0.80$, and excellent if $0.80 < \text{ICC} \leq 1.00$.[21] Bland–Altman plots were also used to present the difference between 2 different measurement methods and the repeated automatic measurement of MRDs. An independent *t* test was used to compare the MPLDs at each angle and analyze the difference between ages and genders. The symmetry of the eyelid contour was evaluated by the temporal-to-nasal MPLD ratios (TNMRs). A *P* value of <0.05 was regarded as statistically significant. All statistical analyses were conducted using SPSS 25.0 (IBM Corporation).

Results

Agreement between Automatic and Manual Measurements

The Dice coefficients of the automatic eyelid and cornea segmentation were 0.929 and 0.936, respectively, demonstrating the robustness of the proposed automatic model (Fig S3, available at www.ophthalmologyscience.org). Manual

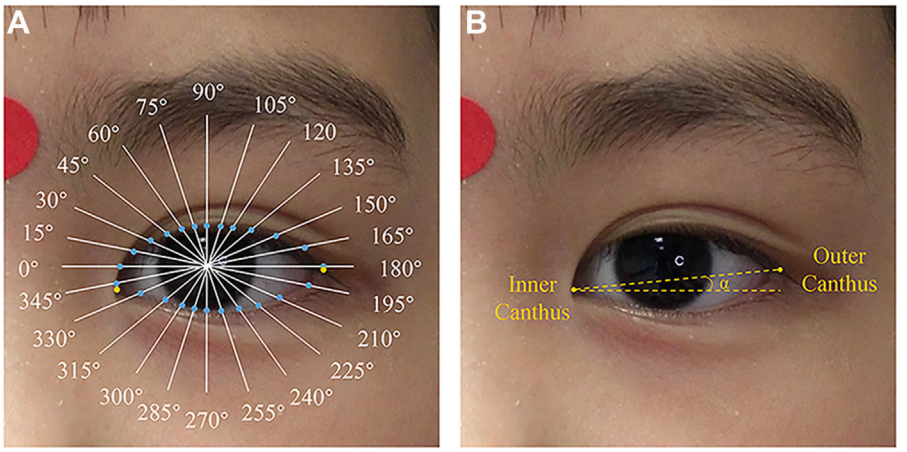

Figure 2. Automatic eyelid measurements. **A,** Midpupil lid distances from 0° to 345°. Twelve radial lines oriented from the pupil center were automatically drawn and intersected the upper and lower eyelid at blue dots. The inner and outer canthi were automatically located at yellow dots. **B,** Palpebral fissure obliquity. A line connecting the inner and outer canthus and a horizontal line across the inner canthus was drawn. The angle (α) between these 2 lines was considered as the palpebral fissure obliquity. This image has been published with the consent of the participant's guardian.

Table 1. Margin Reflex Distances (mean ± SD) Measured by the Automatic and Manual Methods and the Corresponding ICC Between 2 Measurements

	Automatic and Manual (Mm)				Automatic First and Second (Mm)			
	Automatic	*Manual*	*P* Value	ICC	*Automatic First*	*Automatic Second*	*P* Value	ICC
MRD1	2.83 ± 0.40	2.81 ± 0.46	0.466	0.863 (0.840–0.883)*	2.83 ± 0.40	2.83 ± 0.41	0.845	0.970 (0.964–0.974)*
MRD2	3.15 ± 0.60	3.19 ± 0.67	0.300	0.886 (0.866–0.903)*	3.15 ± 0.61	3.15 ± 0.60	0.877	0.986 (0.984–0.988)*

ICC = intraclass correlation coefficient; MRD = margin reflex distance; SD = standard deviation.
*$P < 0.001$.

and repeated automatic measurements of MRDs (mean ± standard deviation) are shown in Table 1. There were excellent agreements between the 2 methods, with ICC being 0.863 (95% confidence interval [CI]: 0.840–0.883, $P < 0.001$) for MRD1 and 0.886 for MRD2 (95% CI: 0.866–0.903, $P < 0.001$) between manual and automatic measurements, 0.970 (95% CI: 0.964–0.974, $P < 0.001$) for MRD1 and 0.986 (95% CI: 0.984–0.988, $P < 0.001$) for MRD2 between 2 repeated automatic measurements. Bland–Altman plots in Figure 4 also confirmed the accuracy and repeatability of the proposed automatic eyelid measurement system. The bias of MRDs ranged from −0.04 to 0.02 between manual and automatic measurements and −0.006 to 0.005 between the 2 repeated automatic measurements.

Eyelid Contour Analysis Using MPLD

Table 2 exhibits all MPLDs from 0° to 345° in males and females of all age groups. From 0° to 180°, the smallest distance appeared at MRD1. Midpupil lid distances gradually increased from the vertical direction toward the horizontal direction and reached the largest value at 180° in all groups. From 195° to 345°, a similar increasing trend of MPLD from vertical to horizontal direction was also observed, with the minimum value at 270° or 285° and the maximum value at 195° or 345°.

Around the horizontal line, most MPLDs in males were significantly greater than that in females ($P < 0.05$). Notably, in the 20s and 30s age groups, female participants had greater MPLDs around the midline (75°–120° in both age groups), whereas male participants had great MPLDs around the horizontal line (0°, 15°, and 330° in the 20s, and 0°, 180°, and 195° in the 30s), and all the differences were statistically significant ($P < 0.05$).

Figures 5 and 6 exhibited the entire eyelid contours in various age groups based on the MPLDs and the location of the canthi. As the age of the participants increased, MPLDs gradually increased at all angles, which peaked in

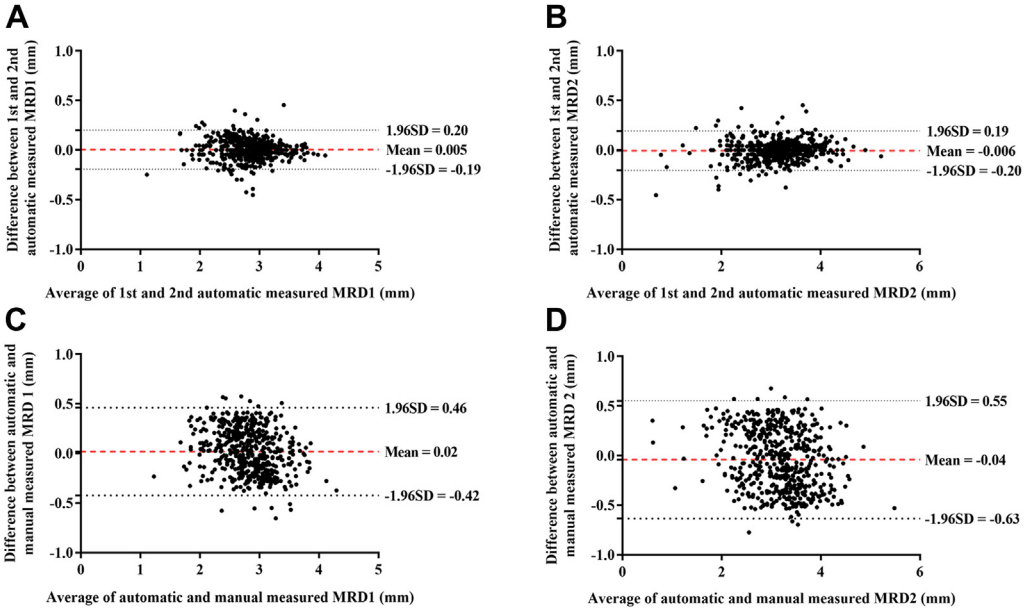

Figure 4. Bland–Altman plots showing excellent agreement between automatically and manually measured margin reflex distances (MRDs). **A,** The differences between 2 repeated automatically measured MRD1. **B,** The differences between 2 repeated automatically measured MRD2. **C,** The differences between automatically and manually measured MRD1. **D,** The differences between automatically and manually measured MRD2. SD = standard deviation; 1st = the first; 2nd = the second.

Table 2. Automatic Eyelid Contour Measurement Using Midpupil Lid Distance (Mm) from 0° to 345° in Different Age Groups

	0–5 Yrs		6–9 Yrs		10–19 Yrs		20–29 Yrs		30–39 Yrs		40–49 Yrs		50–59 Yrs		60–69 Yrs		70–79 Yrs	
Degree	*Male*	*Female*	*Male*	*Female*	*Male*	*Female*	*Male*	*Female*	*Male*	*Female*	*Male*	*Female*	*Male*	*Female*	*Male*	*Female*	*Male*	*Female*
0°	5.79	5.48	5.97	5.80	6.79	6.38*	7.31	6.71*	7.30	6.84†	7.24	6.63‡	7.30	6.36‡	6.15	6.32	6.17	5.77
15°	4.81	4.51*	4.80	4.71	5.28	5.04*	5.55	5.22*	5.53	5.34	5.37	5.11*	5.44	4.95†	4.84	4.87	4.70	4.51
30°	3.95	3.77	3.91	3.86	4.25	4.10	4.40	4.30	4.39	4.37	4.22	4.18	4.32	3.92†	3.82	3.87	3.64	3.56
45°	3.37	3.28	3.37	3.30	3.45	3.42	3.56	3.66	3.55	3.69	3.49	3.47	3.48	3.30	3.14	3.21	3.00	3.05
60°	3.06	2.98	3.06	3.03	3.10	3.11	3.19	3.32	3.17	3.30	3.10	3.09	3.06	2.93	2.78	2.88	2.63	2.78
75°	2.91	2.83	2.93	2.88	2.93	2.94	3.00	3.17*	2.94	3.13*	2.88	2.92	2.83	2.73	2.58	2.67	2.42	2.60
90°	2.91	2.82	2.95	2.92	2.91	2.97	2.99	3.20*	2.92	3.12*	2.85	2.89	2.79	2.68	2.56	2.61	2.41	2.57
105°	3.03	2.95	3.10	3.06	3.00	3.13	3.12	3.32*	3.01	3.19*	2.91	2.97	2.86	2.75	2.61	2.65	2.48	2.60
120°	3.34	3.28	3.47	3.41	3.30	3.45	3.43	3.66*	3.32	3.52*	3.18	3.24	3.11	2.99	2.83	2.87	2.72	2.85
135°	3.98	3.88	4.13	4.10	4.01	4.17	4.21	4.29	3.91	4.12	3.82	3.87	3.64	3.52	3.31	3.36	3.15	3.31
150°	5.17	4.89	5.26	5.19	5.08	5.24	5.41	5.39	5.06	5.13	5.02	4.88	4.69	4.53	4.28	4.23	4.09	4.26
165°	6.74	6.37*	6.99	6.81	6.81	6.88	7.14	6.96	6.73	6.65	6.70	6.43	6.20	5.95	5.76	5.70	5.46	5.49
180°	8.15	7.48‡	8.46	8.14	8.85	8.47*	8.75	8.73	8.88	8.44*	8.43	8.15	7.98	7.74	7.48	7.49	6.52	7.01
195°	6.71	6.03†	6.88	6.60	7.42	7.03	7.33	7.51	7.58	7.08*	6.87	6.48	6.56	6.43	5.91	6.04	5.32	6.00*
210°	5.33	4.88†	5.33	5.19	5.54	5.46	5.64	5.86	5.74	5.52	5.35	5.01	5.14	5.06	4.65	4.69	4.30	4.88*
225°	4.43	4.08*	4.35	4.28	4.42	4.43	4.59	4.78	4.61	4.49	4.31	4.09	4.19	4.12	3.80	3.79	3.56	4.03*
240°	3.83	3.56	3.77	3.71	3.72	3.77	3.93	4.12	3.92	3.88	3.63	3.47	3.61	3.51	3.19	3.20	3.03	3.37
255°	3.42	3.24	3.41	3.40	3.35	3.42	3.55	3.75	3.55	3.49	3.26	3.15	3.22	3.17	2.84	2.91	2.71	3.05
270°	3.33	3.15	3.29	3.26	3.17	3.29	3.40	3.58	3.40	3.38	3.14	3.03	3.09	3.07	2.77	2.86	2.60	2.90
285°	3.33	3.23	3.31	3.30	3.15	3.33	3.47	3.57	3.36	3.42	3.16	3.07	3.14	3.08	2.79	2.87	2.63	2.94
300°	3.57	3.54	3.55	3.51	3.40	3.60	3.73	3.87	3.67	3.71	3.37	3.40	3.40	3.34	3.02	3.15	2.88	3.20
315°	4.20	4.14	4.10	4.10	3.92	4.17	4.27	4.50	4.24	4.30	3.92	3.98	3.96	3.94	3.52	3.71	3.40	3.78
330°	5.21	5.30	5.18	5.26	4.95	5.30*	5.38	5.86*	5.40	5.58	5.03	5.26	4.98	5.13	4.53	4.85	4.28	4.89*
345°	6.68	6.54	6.97	7.09	7.79	7.60	8.57	8.61	9.00	8.64	8.15	8.70	8.24	8.68	7.93	8.55	6.74	7.76

*$P < 0.05$.
†$P < 001$.
‡$P < 0.001$.

the 20s or 30s age group, and then decreased with advancing age. A comparison of MPLDs at the same angle between the 20s and other age groups was conducted (Table 3). For male participants, MPLDs grew before the 20s and the mean difference was statistically significant in the sector near inner canthus. There was a significant decrease in MPLDs in the temporal sector between the 20s and the 50s, and the scope expanded to almost all angles in the 60s and 70s. More angles with significant differences appeared for female participants than for male subjects.

Eyelid Symmetric Analysis Using TNMR

The TNMRs for males and females in all age groups are listed in Table 4. In the upper eyelid, almost all ratios were >1, demonstrating that the temporal sector was larger than the nasal sector. The maximum value of TNMR was at 180/0 or 165/15, and the difference between these 2 values was not significant in all groups (all $P > 0.05$). Generally, TNMRs were smaller from the horizontal line to the midline. In the lower eyelid, TNMRs ranged from 1.02 to 1.13 in males and 0.93 to 1.07 in females.

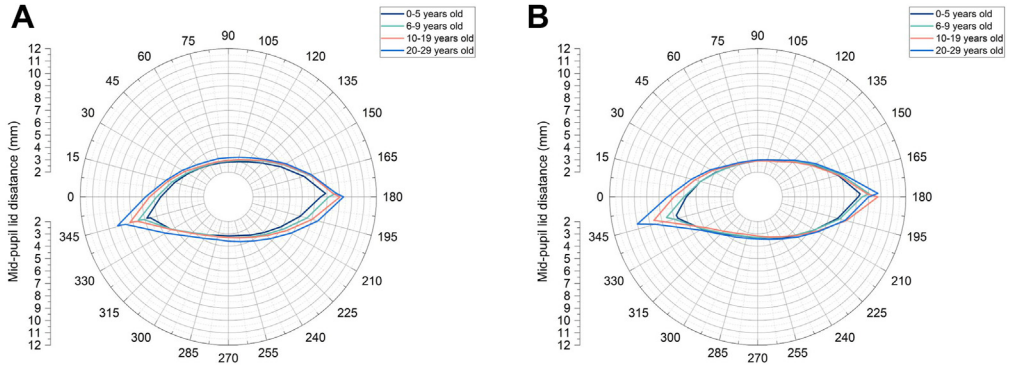

Figure 5. Eyelid contours of the left eye in participants aged 0 to 29 years were automatically drawn. **A,** Eyelid contours in female participants; **B,** Eyelid contours in male participants.

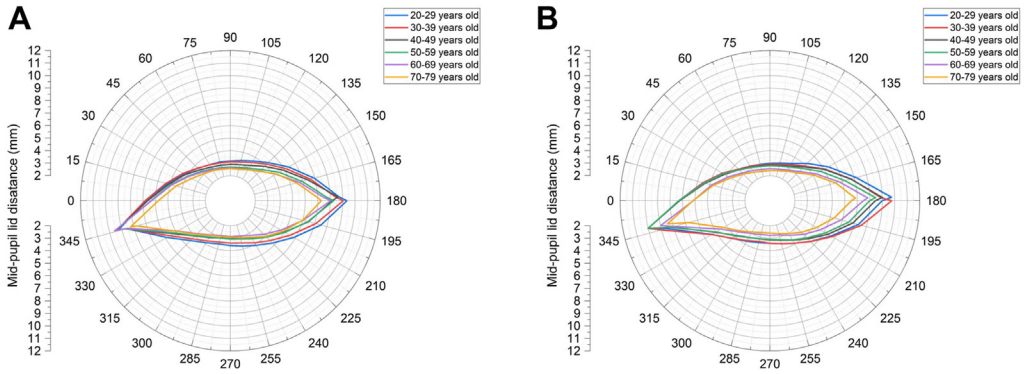

Figure 6. Eyelid contours of the left eye of participants aged 20 to 79 years were automatically drawn. **A,** Eyelid contours in female participants; **B,** Eyelid contours in male participants.

When TNMRs in different age groups were compared with the 20s age group, the statistical difference was mainly in the upper eyelid for both males and females. When compared by gender, most values of TNMRs in the lower eyelid before the 50s were greater for males than females ($P < 0.05$).

Palpebral Fissure Obliquity Analysis

For all groups, the location of the outer canthus ranged from 176° to 183°, whereas the inner canthus ranged from 345° to 352°. This indicated that the outer canthus was higher than the inner canthus for both males and females. As shown in Table 5, palpebral fissure obliquity was larger in females than males at all ages, and the differences were significant in the 0 to 5 years, the 40s, and 50s groups ($P < 0.05$). There was no significant difference in palpebral fissure obliquity after the 20s (Table 6, $P > 0.05$).

Discussion

In this study, we proposed a fully automatic system to quantitatively, quickly, and comprehensively analyze eyelid contour by accurately measuring MPLDs. The results showed that

Table 3. Mean Difference of Midpupil Lid Distance in Different Age Groups Compared with the 20s Age Group

	20s vs. 0–5 Yrs		20s vs. 6–9 Yrs		20s vs. 10s		20s vs. 30s		20s vs. 40s		20s vs. 50s		20s vs. 60s		20s vs. 70s	
Degree	*Male*	*Female*	*Male*	*Female*	*Male*	*Female*	*Male*	*Female*	*Male*	*Female*	*Male*	*Female*	*Male*	*Female*	*Male*	*Female*
0°	1.52‡	1.23‡	1.34‡	0.90‡	0.52†	0.33	0.01	−0.13	0.07	0.08	0.01	0.35	1.16‡	0.39*	1.14‡	0.94‡
15°	0.74‡	0.71‡	0.75‡	0.50‡	0.27*	0.18	0.02	−0.12	0.18	0.11	0.11	0.26*	0.71‡	0.35*	0.84‡	0.71‡
30°	0.46‡	0.52‡	0.49‡	0.44‡	0.15	0.20	0.01	−0.08	0.19	0.12	0.08	0.38‡	0.58‡	0.43‡	0.76‡	0.74‡
45°	0.19*	0.38‡	0.19	0.35‡	0.11	0.24†	0.01	−0.03	0.07	0.19	0.08	0.36‡	0.42‡	0.45‡	0.55‡	0.61‡
60°	0.13	0.33‡	0.12	0.29‡	0.09	0.21*	0.02	0.01	0.09	0.22*	0.13	0.39‡	0.41‡	0.44‡	0.56‡	0.54‡
75°	0.09	0.34‡	0.05	0.28‡	0.06	0.23†	0.05	0.05	0.12	0.25†	0.17	0.44‡	0.42‡	0.51‡	0.57‡	0.57‡
90°	0.08	0.38‡	0.06	0.29‡	0.09	0.24†	0.07	0.09	0.14	0.31‡	0.20*	0.52‡	0.43‡	0.59‡	0.58‡	0.63‡
105°	0.09	0.38‡	0.02	0.27‡	0.12	0.19*	0.11	0.14	0.20*	0.35‡	0.26†	0.57‡	0.51‡	0.67‡	0.64‡	0.72‡
120°	0.09	0.38‡	−0.04	0.25†	0.13	0.20*	0.11	0.14	0.26†	0.42‡	0.32‡	0.67‡	0.60‡	0.79‡	0.71‡	0.81‡
135°	0.23	0.41‡	0.08	0.20	0.21	0.13	0.30*	0.18	0.39‡	0.42‡	0.57‡	0.77‡	0.90‡	0.94‡	1.06‡	0.98‡
150°	0.23	0.50‡	0.14	0.20	0.33*	0.14	0.35†	0.26	0.39†	0.50‡	0.71‡	0.85‡	1.12‡	1.16‡	1.32‡	1.12‡
165°	0.40	0.59‡	0.15	0.15	0.33*	0.08	0.41*	0.31	0.44*	0.53‡	0.94‡	1.01‡	1.38‡	1.25‡	1.68‡	1.46‡
180°	0.60	1.25‡	0.52*	0.59‡	−0.10	0.26	−0.13	0.29	0.31	0.58‡	0.77‡	0.99‡	1.27‡	1.24‡	2.23‡	1.71‡
195°	0.62	1.47‡	0.46	0.91‡	−0.08	0.48*	−0.25	0.43*	0.46	1.03‡	0.78*	1.08‡	1.42‡	1.47‡	2.01‡	1.51‡
210°	0.31	0.99‡	0.31	0.68‡	0.10	0.41†	−0.10	0.34*	0.28	0.85‡	0.50	0.81‡	0.99‡	1.18‡	1.34‡	0.99‡
225°	0.16	0.70‡	0.23	0.50‡	0.17	0.35†	−0.02	0.28*	0.28	0.68‡	0.40	0.66‡	0.79‡	0.98‡	1.02‡	0.75‡
240°	0.10	0.55‡	0.16	0.41‡	0.21	0.34†	0.01	0.23*	0.29	0.65‡	0.32	0.60‡	0.74‡	0.92‡	0.90‡	0.74‡
255°	0.14	0.51‡	0.15	0.35‡	0.21	0.33†	0.00	0.26†	0.29	0.60‡	0.34	0.58‡	0.72‡	0.85‡	0.84‡	0.70‡
270°	0.07	0.43‡	0.11	0.32‡	0.23	0.29†	0.00	0.20*	0.26	0.55‡	0.30	0.51‡	0.63‡	0.72‡	0.80‡	0.68‡
285°	0.14	0.35†	0.16	0.27*	0.32	0.25*	0.10	0.16	0.30	0.50‡	0.33	0.49‡	0.68‡	0.70‡	0.84‡	0.63‡
300°	0.16	0.33*	0.19	0.36‡	0.33	0.28*	0.06	0.17	0.36	0.48‡	0.34	0.53‡	0.72‡	0.72‡	0.85‡	0.67‡
315°	0.06	0.36†	0.16	0.40‡	0.35	0.33†	0.03	0.20	0.35	0.52‡	0.31	0.56‡	0.75‡	0.79‡	0.87‡	0.72‡
330°	0.17	0.56‡	0.20	0.61‡	0.43	0.57‡	−0.02	0.28	0.34	0.60‡	0.40	0.73‡	0.84‡	1.01‡	1.10‡	0.97‡
345°	1.89‡	2.07‡	1.60‡	1.53‡	0.78*	1.01‡	−0.43	−0.03	0.42	−0.08	0.33	−0.06	0.65	0.06	1.84‡	0.86

*$P < 0.05$.
†$P < 0.01$.
‡$P < 0.001$.

Table 4. Temporal-to-Nasal Midpupil Lid Distance Ratio in Different Age and Gender Groups

	0–5 Yrs		6–9 Yrs		10–19 Yrs		20–29 Yrs		30–39 Yrs		40–49 Yrs		50–59 Yrs		60–69 Yrs		70–79 Yrs	
	Male	*Female*	*Male*	*Female*	*Male*	*Female*	*Male*	*Female*	*Male*	*Female*	*Male*	*Female*	*Male*	*Female*	*Male*	*Female*	*Male*	*Female*
Upper Eyelid																		
180°/0°	1.42	1.38	1.43	1.41	1.31	1.34	1.22	1.31	1.22	1.25	1.19	1.23	1.12	1.23	1.27	1.19	1.07	1.24
165°/15°	1.42	1.43	1.48	1.46	1.29	1.39	1.30	1.35	1.22	1.25	1.25	1.26	1.16	1.21	1.21	1.19	1.16	1.25
150°/30°	1.33	1.31	1.36	1.36	1.20	1.30	1.24	1.26	1.16	1.18	1.20	1.18	1.10	1.18	1.14	1.11	1.13	1.23
135°/45°	1.19	1.19	1.24	1.25	1.16	1.23	1.19	1.18	1.11	1.12	1.10	1.12	1.06	1.07	1.06	1.05	1.05	1.10
120°/60°	1.09	1.10	1.14	1.13	1.07	1.12	1.08	1.11	1.05	1.07	1.03	1.05	1.02	1.02	1.02	1.00	1.04	1.03
105°/75°	1.04	1.04	1.06	1.06	1.02	1.06	1.04	1.05	1.02	1.02	1.01	1.02	1.01	1.01	1.01	0.99	1.02	1.01
Lower Eyelid																		
210°/330°	1.03	0.93	1.03	0.99	1.13	1.04	1.04	1.00	1.07	1.00	1.08	0.97	1.05	0.99	1.06	0.98	1.03	1.01
225°/315°	1.06	0.99	1.06	1.04	1.13	1.07	1.07	1.06	1.09	1.05	1.10	1.04	1.07	1.05	1.10	1.03	1.06	1.07
240°/300°	1.07	1.01	1.06	1.06	1.10	1.05	1.05	1.07	1.07	1.05	1.08	1.03	1.07	1.05	1.06	1.02	1.06	1.06
255°/285°	1.03	1.00	1.03	1.03	1.07	1.03	1.02	1.05	1.06	1.02	1.03	1.03	1.03	1.03	1.02	1.01	1.03	1.03

the automatic MRDs were in excellent agreement with the manual MRDs measured by an oculoplastic expert. This automatic image analysis system could be considered a reliable tool for measuring eyelid contour and these detailed eyelid contour parameters of normal individuals in various age and gender groups could serve as a guide for eyelid surgery.

Digital facial images have been utilized to analyze numerical eyelid contour features or analyze surgical outcomes for research purposes.[22–24] Midpupil lid distance, describing the radial distances between the pupil center and lid margins every 15°,[7] were applied to quantize the severity of eyelid contour abnormality and analyze surgical outcomes.[5,7,25] Although the radial lines could be generated by image software, the location of the pupil center and each intersection of the radial line and eyelid still required manual identification, which was time-consuming. Recently, the Bezier curve was used as a new approach to analyzing eyelid contour.[8,26] It simplified the manual annotation process of intersections by adjusting Bezier lines to the lid margins. However, the location of the pupil center and the adjustments of Bezier curves were performed manually, and the need for these human processes makes the process more labor-intensive and may introduce errors. The eyelid contour measurement method in this study was fully automatic and thus had the distinct advantages of having less interobserver variability and being more user-friendly than those semiautomatic methods. The DL-based system comprises 3 automatic steps: eye recognition, eye segmentation, and eyelid contour measurements. The processing time of each participant took <3 seconds from the image input to the output of measured results, eliminating the need for any manual intervention by clinicians. The high ICCs of 2 repeated automatic measurements, up to 0.970, also demonstrated the great repeatability of the automatic system.

Aging could affect both the upper and lower eyelids. A gradual descent of the upper eyelid was frequently reported in the previous studies,[1,27,28] which was also consistent with our findings. However, the influence of aging in the lower eyelid showed conflicting results. Van den Bosch et al[29] showed sagging of the lower eyelid in both genders, which especially occurred in males. Contrarily, the average rise rather than fall of the lower eyelid was reported by several studies.[27,30–32] Age-related position change of the lower eyelid may result from multiple factors. Globe position changes as the increasing diameter of the orbit rim with age, orbital and periorbital fat atrophy, and stretching of the eyes' suspensory ligament contribute to senile enophthalmos.[33,34] Globe retrusion can sink the eyes and narrow the palpebral fissure.[33] Meanwhile, laxity of skin,[35] forward herniation of infraorbital fat,[36,37] and the traction on the lid caused by the loss of the deep cheek fat compartments[38] lead to the sagging of the lower eyelid. In the present study, MPLDs of all angles of the lower eyelid significantly decreased at all angles in the age groups of the 60s and 70s, indicating that the effect of narrowing the palpebral fissure in Chinese may be stronger than that of sagging.

Table 5. Palpebral Fissure Obliquity of Participants

Age (Yrs)	Male (°)	Female (°)	*P* Value
0–5	6.55	8.39	0.022
6–9	7.25	8.29	0.169
10–19	5.18	6.62	0.072
20–29	6.73	6.67	0.919
30–39	5.74	6.39	0.387
40–49	6.10	7.80	0.017
50–59	5.87	7.38	0.018
60–69	6.50	6.95	0.572
70–79	6.10	6.90	0.431

Table 6. Palpebral Fissure Obliquity in Different Age Groups Compared with That in the 20s Age Group

Age Group	Male (°)	*P* value	Female (°)	*P* Value
0–5 yrs vs. 20s	−0.18	0.803	1.71	0.011
6–9 yrs vs. 20s	0.52	0.474	1.61	0.010
10s vs. 20s	−1.56	0.029	−0.05	0.943
30s vs. 20s	−1.00	0.154	−0.28	0.665
40s vs. 20s	−0.63	0.359	1.13	0.062
50s vs. 20s	−0.87	0.172	0.71	0.226
60s vs. 20s	−0.23	0.768	0.27	0.643
70s vs. 20s	−0.63	0.486	0.22	0.761

Quantification of eyelid contour, especially the temporal sector, is essential for objective assessment of blepharoplasty. Studies showed greater temporal hooding in severe congenital blepharoptosis,[39] and obvious temporal eyelid retraction (lateral flare sign) in thyroid-associated ophthalmopathy.[40,41] However, the number of normal participants in previous research was limited, and the MPLD study focused only on adults. The present study reported MPLDs and TNMRs at all angles, not only in adults but also in children. In the literature, 3 studies[1,42,43] showed the peak of TNMR at 180:0 and a gradual decrease from the horizon direction toward the vertical direction. In this study, the overall decrease in the tendency of TNMR from 165:15 to 105:75 was the same as in the previous studies. The division between our study and the previous 3 articles is that the peak of TNMR appeared not only at 180:0 but also at 165:15. However, the differences were not statistically significant in all groups (all $P > 0.05$). A possible explanation for this might be the variances in the location of the lateral canthus. Compared with ending below 180° in the past 3 articles, the lateral canthus, located between 176° to 183° in this study, may slightly increase the steepness of temporal eyelid contour and result in a small rise of asymmetry at 165:15.

The previous research reported contradictory results on the relationship between age, gender, and palpebral fissure obliquity. Gifford[44] concluded from a large number of image measurements that the Asian slant was the illusion of an epicanthal fold and asymmetric narrowing of the palpebral fissure. Park et al[28] reported that the palpebral fissure slant reached a peak between 10 and 13 years and then gradually decreased, with a greater decrease in females. Lee et al[1] found a significantly greater palpebral fissure obliquity in females than in males. This value showed no significant changes after the 20s and a similar result was reported by Ma et al.[27] In a Chinese population study, Cai et al[45] reported a significant increase of the palpebral fissure obliquity from 7.34° in individuals aged 7 to 10 years to 9.72° among those in their 20s. In the present study, we found that the values of the palpebral fissure obliquity were greater in females than males, but significant differences were only found in the age groups of 0 to 5 years, the 40s, and 50s. The peak level appeared before 10 years in both genders and remained relatively stable after the 20s.

This study had the following limitations. First, although we recruited 540 normal individuals aged 0 to 79 years of both genders, this was a single-center study and all participants were Chinese. Further work is warranted to explore the shape of the eyelid in different ethnic groups and recruit a larger number of participants in different medical institutions. Second, this work is a proof-of-concept. We are working on the validation of the reproducibility and stability of the proposed system in multicenters and are planning to develop and release a user-friendly app. Third, though the manual measurements were performed by an ocular plastic expert with >15 years of experience, the reliability of manual measurements would be enhanced when applying the average value obtained from 3 experienced ophthalmologists. Fourthly, the photographic technology was 2-dimensional. Without the consideration of the anteroposterior dimension of the eye, the values of MPLDs may not fully quantify the eyelid contour. Therefore, we are also planning to further analyze eyelid features in 3-dimensional photography.

In conclusion, we proposed an objective, quick, and fully automatic lid system to measure the contour of the entire eyelid, and compared these contours according to different gender and age groups. Being aware of the quantitative and comprehensive eyelid features in normal individuals may help in the objective evaluation of eyelid reconstruction and rejuvenation surgery.

Footnotes and Disclosures

Originally received: October 18, 2023.
Final revision: March 3, 2024.
Accepted: March 12, 2024.
Available online: March 21, 2024. Manuscript no. XOPS-D-23-00266R1.

Eye Center, The Second Affiliated Hospital, School of Medicine, Zhejiang University, Zhejiang Provincial Key Laboratory of Ophthalmology, Zhejiang Provincial Clinical Research Center for Eye Diseases, Zhejiang Provincial Engineering Institute on Eye Diseases, Hangzhou, Zhejiang, China.

*J.S. and J.C. contributed equally to this work.

Disclosure(s):

All authors have completed and submitted the ICMJE disclosures form.

The authors have no proprietary or commercial interest in any materials discussed in this article.

Supported by the National Natural Science Foundation Regional Innovation and Development Joint Fund (grant no.: U20A20386 [to J.Y.]), National Natural Science Foundation of China (grant no.: 82000948 [to L.L.]), National Key Research and Development Program of China (grant no.: 2019YFC0118400 [to J.Y.]), National Natural Science Foundation of China (grant no.: 82101178 [to C.W.]). The sponsor or funding organization had no role in the design or conduct of this research.

HUMAN SUBJECTS: Human subjects were included in this study. The study was conducted in accordance with the Declaration of Helsinki and was approved by the Ethics Committees of the Second Affiliated Hospital of Zhejiang University, School of Medicine (Approval No. 2020-583) and registered with ClinicalTrials.gov (No. NCT04921020). Informed consent was obtained from all adult participants and guardians of minors.

No animal subjects were used in this study.

Author Contributions:

Conception and design: Shao, Cao, Lou, Ye

Data collection: Shao, Cao

Analysis and interpretation: Shao, Wang, Xu

Obtained funding: Wang, Lou, Ye

Overall responsibility: Shao, Cao, Wang, Xu, Lou, Ye

Abbreviations and Acronyms:
CI = confidence interval; **DL** = deep learning; **ICC** = intraclass correlation coefficient; **MPLD** = midpupil lid distance; **MRD** = margin reflex distance; **TNMR** = temporal-to-nasal midpupil lid distance ratio.

Keywords:
Automatic measurement, Deep learning, Eyelid contour, Facial images.

Correspondence:
Juan Ye, MD, PhD; Lixia Lou, MD, PhD; No. 1 Xihu Road, Eye Center, The Second Affiliated Hospital, School of Medicine, Zhejiang University, Zhejiang Provincial Key Laboratory of Ophthalmology, Zhejiang Provincial Clinical Research Center for Eye Diseases, Zhejiang Provincial Engineering Institute on Eye Diseases, Hangzhou, Zhejiang Province, China. E-mail: yejuan@zju.edu.cn; loulixia110@zju.edu.cn.

References

1. Lee H, Lee JS, Chang M, et al. Analysis of lid contour change with aging in Asians by measuring midpupil lid distance. *Plast Reconstr Surg*. 2014;134:521e−529e. https://doi.org/10.1097/PRS.0000000000000579.
2. Patil SB, Kale SM, Math M, et al. Anthropometry of the eyelid and palpebral fissure in an Indian population. *Aesthet Surg J*. 2011;31:290−294. https://doi.org/10.1177/1090820X11398475.
3. Noh SH, Choi U. The palpebral fissure of the Korean youth. *J Korean Ophthalmol Soc*. 1981;22:497−498.
4. Golbert M, Pereira FJ, Garcia DM, Cruz AAV. Contour symmetry of the upper eyelid following bilateral conjunctival-Müller's muscle resection. *Aesthet Surg J*. 2017;37:269−275. https://doi.org/10.1093/asj/sjw242.
5. Ribeiro SFT, Milbratz GH, Garcia DM, et al. Pre- and postoperative quantitative analysis of contour abnormalities in graves upper eyelid retraction. *Ophthal Plast Reconstr Surg*. 2012;28:429−433. https://doi.org/10.1097/IOP.0b013e3182696532.
6. Cruz AAV, Equitério B, Diniz SB, et al. Upper eyelid contour changes after orbital decompression in Graves orbitopathy. *Ophthal Plast Reconstr Surg*. 2022;38:289−293. https://doi.org/10.1097/IOP.0000000000002093.
7. Milbratz GH, Garcia DM, Guimarães FC, Cruz AA. Multiple radial midpupil lid distances: a simple method for lid contour analysis. *Ophthalmology*. 2012;119:625−628. https://doi.org/10.1016/j.ophtha.2011.08.039.
8. Huelin FJ, Sales-Sanz M, Ye-Zhu C, et al. Bezier curves as a total approach to measure the upper lid contour: redefining clinical outcomes in palpebral surgery. *Br J Ophthalmol*. 2023;107:6−11. https://doi.org/10.1136/bjophthalmol-2021-319666.
9. Huang X, Li Z, Lou L, et al. GOMPS: global attention-based ophthalmic image measurement and postoperative appearance prediction system. *Expert Syst Appl*. 2023;232:120812. https://doi.org/10.1016/j.eswa.2023.120812.
10. Lee A, Taylor P, Kalpathy-Cramer J, Tufail A. Machine learning has arrived. *Ophthalmology*. 2017;124:1726−1728. https://doi.org/10.1016/j.ophtha.2017.08.046.
11. Lou L, Cao J, Wang Y, et al. Deep learning-based image analysis for automated measurement of eyelid morphology before and after blepharoptosis surgery. *Ann Med*. 2021;53:2278−2285. https://doi.org/10.1080/07853890.2021.2009127.
12. Jin K, Ye J. Artificial intelligence and deep learning in ophthalmology: current status and future perspectives. *Adv Ophthalmol Pract Res*. 2022;2:100078. https://doi.org/10.1016/j.aopr.2022.100078.
13. Shao J, Huang X, Gao T, et al. Deep learning-based image analysis of eyelid morphology in thyroid-associated ophthalmopathy. *Quant Imaging Med Surg*. 2023;13:1592−1604. https://doi.org/10.21037/qims-22-551.
14. Putterman AM. Margin reflex distance (MRD) 1, 2, and 3. *Ophthal Plast Reconstr Surg*. 2012;28:308−311. https://doi.org/10.1097/IOP.0b013e3182523b7f.
15. Zuo Q, Chen S, Wang Z. R2AU-net: attention recurrent residual convolutional neural network for multimodal medical image segmentation. *Sec Commun Netw*. 2021;2021:1−10. https://doi.org/10.1155/2021/6625688.
16. Cai Y, Zhang X, Cao J, et al. Application of artificial intelligence in oculoplastics. *Clin Dermatol*. 2024. https://doi.org/10.1016/j.clindermatol.2023.12.019.
17. Cao J, Lou L, You K, et al. A novel automatic morphologic analysis of eyelids based on deep learning methods. *Curr Eye Res*. 2021;46:1495−1502. https://doi.org/10.1080/02713683.2021.1908569.
18. Yin XX, Sun L, Fu Y, Lu R, Zhang Y. U-net-based medical image segmentation. *J Healthc Eng*. 2022;2022. https://doi.org/10.1155/2022/4189781.
19. Liu Z, Luo P, Wang X, Tang X. Deep learning face attributes in the wild. IEEE International Conference on Computer Vision (ICCV). Chile: IEEE *Santiago*. 2015:3730−3738. https://doi.org/10.1109/ICCV.2015.425.
20. Ghassabeh YA. A sufficient condition for the convergence of the mean shift algorithm with Gaussian kernel. *J Multivariate Anal*. 2015;135:1−10. https://doi.org/10.1016/j.jmva.2014.11.009.
21. Landis JR, Koch GG. The Measurement of observer agreement for categorical data. *Biometrics*. 1977;33:159−174. https://doi.org/10.2307/2529310.
22. Cruz AAV, Coelho RP, Baccega A, et al. Digital image processing measurement of the upper eyelid contour in Graves disease and congenital blepharoptosis. *Ophthalmology*. 1998;105:913−918. https://doi.org/10.1016/S0161-6420(98)95037-0.
23. Lou L, Yang L, Ye X, et al. A novel approach for automated eyelid measurements in blepharoptosis using digital image analysis. *Curr Eye Res*. 2019;44:1075−1079. https://doi.org/10.1080/02713683.2019.1619779.
24. Bahçeci Şimşek İ, Şirolu C. Analysis of surgical outcome after upper eyelid surgery by computer vision algorithm using face and facial landmark detection. *Graefes Arch Clin Exp Ophthalmol*. 2021;259:3119−3125. https://doi.org/10.1007/s00417-021-05219-8.
25. Gonçalves ACP, Nogueira T, Gonçalves ACA, et al. A comparative study of full-thickness blepharotomy versus transconjunctival eyelid lengthening in the correction of upper eyelid retraction in Graves' orbitopathy. *Aesthet Plast Surg*. 2018;42:215−223. https://doi.org/10.1007/s00266-017-0978-9.
26. Sales-Sanz M, Huelin FJ, Ye-Zhu C, et al. Müllerotomy with anterior graded Müller muscle disinsertion for Graves upper eyelid retraction: validation of surgical outcomes using Bézier curves. *Graefes Arch Clin Exp Ophthalmol*. 2023;261:1141−1149. https://doi.org/10.1007/s00417-022-05853-w.
27. Ma H, Chen Y, Cai X, et al. Effect of aging in periocular appearances by comparison of anthropometry between early and middle adulthoods in Chinese Han population. *J Plast Reconstr Aesthet Surg*. 2019;72:2002−2008. https://doi.org/10.1016/j.bjps.2019.07.030.
28. Park DH, Choi WS, Yoon SH, Song CH. Anthropometry of Asian eyelids by age. *Plast Reconstr Surg*. 2008;121:1405−1413. https://doi.org/10.1097/01.prs.0000304608.33432.67.

29. van den Bosch WA, Leenders I, Mulder P. Topographic anatomy of the eyelids, and the effects of sex and age. *Br J Ophthalmol*. 1999;83:347−352. https://doi.org/10.1136/bjo.83.3.347.
30. Lambros V, Amos G. Three-dimensional facial averaging: A tool for understanding facial aging. *Plast Reconstr Surg*. 2016;138:980e−982e. https://doi.org/10.1097/PRS.0000000000002752.
31. Rana K, Beecher MB, Caltabiano C, et al. Normal periocular anthropometric measurements in an Australian population. *Int Ophthalmol*. 2023;43:2695−2701. https://doi.org/10.1007/s10792-023-02669-3.
32. Yang E, Xinhao L, Hengshu Z. Analysis of aging-related changes in the lower eyelid tissue structure in Han Chinese women. *J Plast Reconstr Aesthet Surg*. 2022;75:3420−3428. https://doi.org/10.1016/j.bjps.2022.04.095.
33. Athanasiov PA, Prabhakaran VC, Selva D. Non-traumatic enophthalmos: a review. *Acta Ophthalmol*. 2008;86:356−364. https://doi.org/10.1111/j.1755-3768.2007.01152.x.
34. Kahn DM, Shaw RB. Overview of current thoughts on facial volume and aging. *Facial Plast Surg*. 2010;26:350−355. https://doi.org/10.1055/s-0030-1265024.
35. Swift A, Liew S, Weinkle S, et al. The facial aging process from the "inside out". *Aesthet Surg J*. 2021;41:1107−1119. https://doi.org/10.1093/asj/sjaa339.
36. Richard MJ, Morris C, Deen BF, et al. Analysis of the anatomic changes of the aging facial skeleton using computer-assisted tomography. *Ophthalmic Plast Reconstr Surg*. 2009;25:382−386. https://doi.org/10.1097/IOP.0b013e3181b2f766.
37. Lee JM, Lee H, Park M, et al. The volumetric change of orbital fat with age in Asians. *Ann Plast Surg*. 2011;66:192−195. https://doi.org/10.1097/SAP.0b013e3181e6d052.
38. Pessa JE. An algorithm of facial aging: verification of Lambros's theory by three-dimensional stereolithography, with reference to the pathogenesis of midfacial aging, scleral show, and the lateral suborbital trough deformity. *Plast Reconstr Surg*. 2000;106:479−490. https://doi.org/10.1097/00006534-200008000-00040.
39. Cruz AA, Lucchezi MC. Quantification of palpebral fissure shape in severe congenital blepharoptosis. *Ophthal Plast Reconstr Surg*. 1999;15:232−235. https://doi.org/10.1097/00002341-199907000-00002.
40. Ribeiro SFT, Milbratz GH, Garcia DM, et al. Lateral and medial upper eyelid contour abnormalities in Graves orbitopathy: the influence of the degree of retraction. *Ophthal Plast Reconstr Surg*. 2013;29:40−43. https://doi.org/10.1097/IOP.0b013e3182747537.
41. Equiterio BS, Garcia DM, Cruz AA, et al. Lid flare measurement with lateral midpupil distances. *Curr Eye Res*. 2021;46:1309−1313. https://doi.org/10.1080/02713683.2021.1878541.
42. Kang D, Lee J, Park J, et al. Analysis of lid contour in thyroid eye disease with upper and lower eyelid retraction using multiple radial midpupil lid distances. *J Craniofac Surg*. 2016;27:134−136. https://doi.org/10.1097/SCS.0000000000001995.
43. Choudhary MM, Chundury R, McNutt SA, Perry JD. Eyelid contour following conjunctival Müllerectomy with or without tarsectomy blepharoptosis repair. *Ophthal Plast Reconstr Surg*. 2016;32:361−365. https://doi.org/10.1097/IOP.0000000000000545.
44. Gifford H. The "Mongolian eye". *Am J Ophthalmol*. 1928;11:887−893. https://doi.org/10.1016/S0002-9394(28)90622-4.
45. Cai X, Chen Y, Li Q, et al. Anthropometric analysis on the ocular region morphology of children and young adults in Chinese Han population. *Ophthal Plast Reconstr Surg*. 2019;35:326−332. https://doi.org/10.1097/IOP.0000000000001245.